

Equilibration and macroscopic quantum fluctuations in the Dicke model

Alexander Altland

Institut für Theoretische Physik, Universität zu Köln, Köln, 50937, Germany

Fritz Haake

Fakultät für Physik, Universität Duisburg-Essen, 47048 Duisburg, Germany

We discuss the unitary quantum dynamics of the Dicke model (spin and oscillator coupled). A suitable quasiprobability representing the quantum state turns out to obey a Fokker-Planck equation, with drift terms representing the underlying classical Hamiltonian flow and diffusion terms describing quantum fluctuations. We show (by projecting the dynamics onto a co-moving Poincaré section) how the interplay of deterministic drift and quantum diffusion generates equilibration to the microcanonical density, under conditions of global classical chaos. The pertinent photon statistics reveals macroscopic quantum fluctuations.

I. INTRODUCTION

The Dicke model [1] has long been known for its quantum phase transition (to a superradiant phase as the coupling exceeds a critical value) [2] and classical as well as quantum chaos [3–5]. New interest in the model has recently been stimulated by an experimental realization (employing a double Bose-Einstein condensate coupled to an electromagnetic mode of a surrounding cavity) where the zero-temperature phase transition was observed [6]. Fascinatingly, a many-body system here exhibits macroscopic quantum behavior involving only two coupled degrees of freedom, one each for spin and oscillator.

The observation of chaos requires a combination of not too small coupling and sufficient excitation. The experimental realization of such regimes would reveal two distinctive signatures of chaos, dissipationless equilibration on the energy shell [7] and macroscopic stationary fluctuations of the photon number, and both of these should be accessible in the condensate/cavity setting of Ref. [6]. For large values of the quantum number j fixing the conserved square of the spin as $\vec{J}^2 = j(j+1) \gg 1$, the quantum dynamics will be strongly influenced by the classical Hamiltonian flow. The essential physics of the Dicke model will thus be governed by an interplay of classical chaos and semiclassical quantum fluctuations.

The purpose of this paper is threefold:

- i) We will present a comprehensive discussion of chaos in the system. Unlike with the pioneering study [5], we will not limit ourselves to the vicinity of the system's ground states but address the full phase space available to chaotic fluctuations.
- ii) We discuss how a conspiracy of quantum fluctuations and nonlinear classical dynamics generates 'thermalization' to a microcanonical distribution. We thus present a first case study where the general role of quantum fluctuations in a chaotic thermalization process is resolved in microscopic detail.
- iii) We will analyse giant fluctuations of observables such as the photon number resulting from the uniform coverage of the system's energy shell.

i) For the classical motion of the Dicke model, we will identify regimes of integrable, mixed and fully chaotic dynamics in regimes of small, intermediate and strong spin-oscillator coupling. Specifically, we will show that chaotic trajectories sweep out large intervals of the classical action variable corresponding to the number of oscillator quanta. The tendency to uniform coverage of the energy shell, typical for dominantly chaotic behavior, arises already for rather moderate energies, provided the coupling is sufficiently large. We conclude the classical discussion by demonstrating that the classical Liouville equation would effectively entail equilibration to the energy shell. The disclaimer 'effectively' refers to the fact that the classical Q evolves into an infinitely rugged distribution of alternating high and zero phase space density. Only in the infinite time limit, the ensuing structure becomes infinitely filigree, and looks homogeneous at any finite resolution.

ii) To describe the quantum dynamics, we represent the density operator by a suitable quasi-probability, the Glauber Q -function aka Husimi function. Schrödinger's equation then turns into a Fokker-Planck equation for Q . The drift terms therein (first-order derivatives) reflect the classical Hamiltonian flow while the second-order derivative terms, small in the parameter $1/j$, describe quantum diffusion. The important role of quantum diffusion is, under conditions of global classical chaos, to limit the shrinking of phase space structures along the classically stable directions to a scale of the order $j^{-1/2}$. The competition of classical vs quantum contraction and expansion of phase space structures corroborates equilibration to the microcanonical distribution. In particular it implies that a) any quasi-probability Q will eventually cover the compact energy shell of the model, on a time scale bounded from above by the Ehrenfest time. Further, our theory reveals explicitly how quantum diffusion smoothens the ruggedness of classical structures over scales $\sim j^{-1/2}$. As a result, we obtain thermalization into a genuinely uniform distribution (to be distinguished from a fissured structure that only looks like a distribution upon decreasing the level of resolution) on time scales of the order of the Ehrenfest time $\sim \ln(j)$.

It is worth emphasizing that the smoothing mechanism relies on the effect of quantum fluctuations *during* the dynamical evolution, rather than just reflecting the *initial* quantum uncertainty intrinsic to any starting distribution.

iii) The ensuing uniform coverage of the energy shell entails large fluctuations of observables such as the photon number or spin projections. The underlying (semiclassical) physics is that during their dynamical evolution, system trajectories fully explore the available phase volume in an essentially unpredictable manner. For instance, in the superradiant regime and at energies $E \gtrsim \hbar\omega_0 j$, where ω_0 is the spin precession frequency, the average photon number is roughly given by $\bar{n} \sim \mathcal{O}(E/\hbar\omega)$. The fluctuations, δn superimposed on this mean are of order $\delta n \sim \mathcal{O}(j^{1/2}\sqrt{\bar{n}}) \sim \mathcal{O}(\bar{n})$, i.e. ‘macroscopic’ fluctuations as big as the average may occur.

The rest of the paper is organized as follows. In Sect. II we discuss the Hamiltonian and the quantum dynamics it generates. Specifically, the quasiprobability Q will be shown to obey a Fokker-Planck equation. Sect. III is devoted to the classical dynamics and in Sect. IV we investigate quantum diffusion. Finally, in Sect. V we discuss fluctuations of the photon number by calculating the microcanonical averages of moments. In Sect. VI we point out why the chaotic drift/diffusion mechanism bringing about equilibration and large stationary fluctuations works in other systems as well. Prominent examples are the kicked top (recently realized experimentally) and the Bose-Hubbard model (a genuine many-body system of much current interest). Appendices will detail some calculations.

II. MODEL AND QUANTUM EVOLUTION

The Hamiltonian of the Dicke model can be written as

$$\hat{H} = \hbar \left\{ \omega_0 \hat{J}_z + \omega a^\dagger a + g \sqrt{\frac{2}{j}} (a + a^\dagger) \hat{J}_x \right\}. \quad (1)$$

Here, the operators $\hat{J}_a, a = x, y, z$ act in a spin- j representation and obey the standard commutation relations $[\hat{J}_a, \hat{J}_b] = i\epsilon_{abc}\hat{J}_c$, where $\{\epsilon_{abc}\}$ is the fully antisymmetric tensor. The photon annihilation and creation operators fulfill the Bose commutation rules $[a, a^\dagger] = 1$. The first two terms in (1) respectively describe spin precession about the J_z -axis with frequency ω_0 and harmonic oscillation with frequency ω . The last term accounts for spin precession about the J_x -axis with a ‘frequency’ $\propto a + a^\dagger$ and for driving of the oscillator by a ‘force’ $\propto J_x$. The coupling constant g is a (Rabi) frequency independent of \hbar . The appearance of the spin quantum number j in the interaction part is owed to the use of the operators a, a^\dagger, \vec{J} which are rather non-classical in character [8]. We note that the Hamiltonian (1) contains the antiresonant terms $J_+ a^\dagger + J_- a$. Only the parity $P = \exp i\pi(a^\dagger a + J_z)$ thus remains as a symmetry. If the antiresonant terms were

dropped (‘rotating wave approximation’), conservation of $a^\dagger a + J_z$ and thus integrability would result.

A. Coherent state representation

We aim to explore the quantum dynamics generated by the Hamiltonian (1). In view of the largeness of the spin, $j \gg 1$, we find it convenient to employ coherent states which are optimally suited to taking semiclassical limits. Specifically, spin coherent states [9–11] are defined as

$$|z\rangle \equiv \frac{1}{(1+|z|^2)^j} e^{z\hat{J}_-} |j, j\rangle, \quad (2)$$

where $|j, j\rangle$ is a ‘maximum-weight’ eigenstate of J_z , i.e. $J_z|j, j\rangle = j|j, j\rangle$. The states $|z\rangle$ yield the mean values

$$\begin{aligned} \langle z | \hat{J}_x | z \rangle &= j \frac{z + z^*}{1 + |z|^2} \equiv j l_x, \\ \langle z | \hat{J}_y | z \rangle &= \frac{j}{i} \frac{z - z^*}{1 + |z|^2} \equiv j l_y, \\ \langle z | \hat{J}_z | z \rangle &= j \frac{1 - |z|^2}{1 + |z|^2} \equiv j l_z; \end{aligned} \quad (3)$$

here $l_{x,y,z}$ are the three components of a unit vector $\mathbf{l} = (\sin\theta \cos\phi, \sin\theta \sin\phi, \cos\theta)^T$, whose angular orientation is defined through $z = e^{i\phi} \tan(\theta/2)$. Higher moments reveal minimum angular uncertainty, characterized by the solid angle $4\pi/(2j+1)$ which defines a Planck cell on the unit sphere. The set $\{|z\rangle\}$ is overcomplete and allows the resolution of unity by $\mathbb{1} = \int dz \frac{2j+1}{\pi(1+zz^*)^2} |z\rangle\langle z|$. Two spin coherent states have the overlap $\langle z | z' \rangle = \frac{(1+z^*z')^{2j}}{(1+|z|^2)^j(1+|z'|^2)^j}$.

Similarly, oscillator coherent states are defined as [12]

$$|\alpha\rangle = e^{-\alpha\alpha^*/2} e^{\alpha a^\dagger} |0\rangle \quad (4)$$

with $\alpha \in \mathbb{C}$ a complex amplitude and $|0\rangle$ the vacuum, $a|0\rangle = 0$. The resolution of unity in terms of the (over)complete set $\{|\alpha\rangle\}$ reads $\mathbb{1} = \frac{1}{\pi} \int d\alpha |\alpha\rangle\langle\alpha|$. The state $|\alpha\rangle$ assigns a minimal uncertainty product to displacement and momentum such that these quantities are ‘confined’ to a single Planck cell. The latter property is also evident from the overlap $|\langle\alpha|\alpha'\rangle|^2 = e^{-|\alpha-\alpha'|^2}$.

We shall discuss the dynamics of the system in terms of its density operator $\hat{\rho}(t)$ and represent the latter by the Glauber Q or Husimi function [11]

$$Q(\alpha, z) = \frac{2j+1}{\pi(1+zz^*)^2} \langle\alpha, z | \hat{\rho} | \alpha, z\rangle. \quad (5)$$

Obviously, that function is real and non-negative everywhere and exists for any density operator $\hat{\rho}$. By invoking the completeness relations given above, one immediately checks that expectation values of (anti-normal ordered) operators of the oscillator can be computed as

$$\langle a^m a^{\dagger n} \rangle = \int d\alpha dz \alpha^m \alpha^{*n} Q(\alpha, z). \quad (6)$$

Expectation values of spin operators can be computed by analogous averaging over z -valued functions. We just note the example

$$\langle a^m a^{\dagger n} \hat{J}_a \rangle = \int d\alpha dz \alpha^m \alpha^{*n} (j+1) l_a(z, z^*) Q(\alpha, z), \quad (7)$$

where the unit increment over j in the factor $(j+1)$ is a quantum correction. At any rate, the foregoing properties of Q allow us to speak of a quasi-probability density which is expected to converge to a classical phase-space density in the limit $\hbar \rightarrow 0$.

To illustrate the use of our quasiprobability we note that a density operator projecting onto a pure coherent state $|z_0, \alpha_0\rangle \equiv |z_0\rangle \otimes |\alpha_0\rangle$ implies a Q -function smeared

$$\begin{aligned} \dot{Q} &= (\mathcal{L} + \mathcal{L}_{\text{diff}})Q \\ \mathcal{L} &= i\partial_\alpha \left(\omega\alpha + g\sqrt{\frac{2}{j}}(j+1)\frac{z+z^*}{1+|z|^2} \right) + i\partial_z \left(-\omega_0 z + \frac{g}{\sqrt{2j}}(1-z^2)(\alpha + \alpha^*) \right) + \text{c.c.}, \quad \mathcal{L}_{\text{diff}} = \frac{ig}{\sqrt{2j}}\partial_\alpha\partial_z(1-z^2) + \text{c.c.}, \end{aligned} \quad (9)$$

and may thus speak of a Fokker-Planck equation. We add in passing that we disregard any damping, restricting ourselves, with respect to the condensate/cavity experiment of Ref. [6], to times smaller than the life times of both the cavity photons and the condensate.

To discuss the semiclassical limit [13] $j \gg 1$, it is convenient to switch to variables obeying canonical classical commutation relations. For the oscillator, we introduce 'action-angle' variables (I, ψ) through [14]

$$\alpha = \sqrt{jI}e^{i\psi}, \quad \alpha^* = \sqrt{jI}e^{-i\psi}. \quad (10)$$

To parametrize the Bloch sphere of the spin we employ $(\cos\theta, \phi)$, cf. (3). Both pairs are canonical, with Poisson brackets $\{I, \psi\} = \{\cos\theta, \phi\} = 1$. A few details pertaining to the change of variables are given in Appendix B.

Expressed in terms of these variables, the drift operator \mathcal{L} assumes the form of a Liouvillian, $\mathcal{L} = -\{h, \}$, with the effective Hamiltonian function

$$h = \omega_0 \cos\theta + \omega I + g\sqrt{8I} \cos\psi \sin\theta \cos\phi, \quad (11)$$

obtained from the Hamilton operator (1) by substituting $\hat{\mathbf{J}} \rightarrow j\mathbf{l}$, $a \rightarrow \sqrt{jI}\exp(i\psi)$, and dividing out $\hbar j = L$. The classical approximation $d_t Q \simeq \mathcal{L}Q = -\{h, Q\}$ to the evolution equation (9) describes a drift of the quasi-probability $Q(I, \psi, \cos\theta, \phi)$ along the classical trajectories of the Hamiltonian flow. The latter are determined

out over a single Planck cell as

$$Q(z, \alpha) = \frac{2j+1}{\pi^2(1+|z|^2)^2} |\langle \alpha, z | \alpha_0, z_0 \rangle|^2. \quad (8)$$

We shall in fact mostly imagine the system initially prepared in such a nearly classical state.

B. Time evolution

The von Neumann equation $d_t \hat{\rho} = \frac{i}{\hbar} [\hat{H}, \hat{\rho}]$ can be rewritten as a partial differential equation for the quasi-probability Q . Using the definition of the coherent states we find (see appendix A) that equation to involve only first and second derivative terms respectively interpretable as classical drift and quantum diffusion,

by the Hamiltonian equations of motion

$$\begin{aligned} \dot{I} &= -\sqrt{8g\sqrt{I}} \sin\psi \sin\theta \cos\phi \\ \dot{\psi} &= -\omega - \sqrt{2g}\frac{1}{\sqrt{I}} \cos\psi \sin\theta \cos\phi \\ \dot{\phi} &= \omega_0 - \sqrt{8g\sqrt{I}} \cos\psi \cot\theta \cos\phi \\ \dot{\cos\theta} &= \sqrt{8g\sqrt{I}} \cos\psi \sin\theta \sin\phi. \end{aligned} \quad (12)$$

As befits classical Hamiltonian equations the quantum number j does not show up here.

When the quantum diffusion operator $\mathcal{L}_{\text{diff}}$ is written in terms of the above canonical pairs of variables, it acquires a pre-factor $\frac{1}{j}$ which is very small in the semiclassical limit. That semiclassical smallness notwithstanding, quantum diffusion has an important smoothing effect on the quasi-probability Q , as we shall see presently. But first, we devote a thorough discussion to the drift.

III. CLASSICAL DYNAMICS

In this section, we will analyse the phase space flow according to the classical Hamiltonian equations (12), in regimes of integrable, chaotic, and mixed dynamics. A discussion of chaos in the system has been reported in a seminal paper by Brandes and Emary [5]. However, the Holstein-Primakoff bosons employed to represent the spin variables in that reference tend to obscure the large-scale phase-space structure of the problem, and notably the semiclassical limits $j \rightarrow \infty$ and $\hbar \rightarrow 0$ at $\hbar j \equiv L = \text{const}$. For an insightful discussion of chaos in the equations of

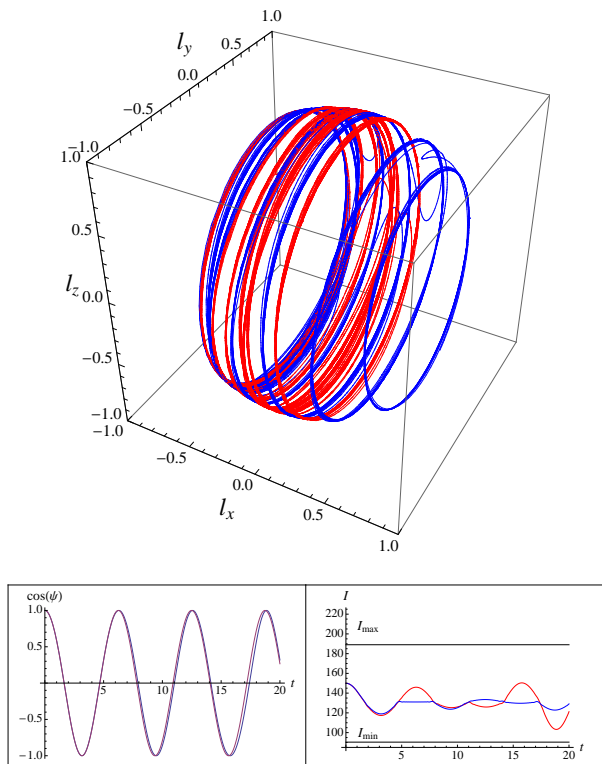


FIG. 1. Chaotic trajectories of the classical Dicke model at $g = 3g_c$ and $h \simeq 150\omega_0$. The red and the blue trajectory differ in a slight mismatch of the initial conditions.

motion (12) (applied to an opto-mechanical setting) we also refer to Ref. [15]. The primary objective of our classical analysis is to set the stage for the discussion of the quantum ramifications of chaos.

A. Qualitative picture

The equations of motion (12) do not involve the quantum parameters \hbar and $j = L/\hbar$. Remarkably, the scaled Hamiltonian h is also independent of the classical angular momentum $L = j\hbar$, due to the particular scaling (10) of the oscillator variables. Put differently, the magnitude of the classical angular momentum does not affect the dynamics and can be accommodated in a rescaling of variables. The dynamics then depends on the dimensionless measures for frequency, coupling, and energy

$$\nu \equiv \frac{\omega}{\omega_0}, \quad \gamma \equiv \frac{g}{g_c}, \quad \epsilon \equiv h/\omega_0, \quad (13)$$

with $g_c \equiv \sqrt{\omega\omega_0}/2$ the critical coupling at which the Dicke model undergoes its transition to a superradiant phase. Without much loss of generality, we will assume comparable frequencies $\omega/\omega_0 = \mathcal{O}(1)$ throughout[16]. To obtain some intuition of the dynamics, let us express the Hamiltonian in terms of the unit-length angular momen-

tum $\mathbf{l} = (l_x, l_y, l_z)$:

$$\frac{h}{\omega_0} = l_z + \nu I + \gamma\sqrt{2\nu I} \cos \psi l_x, \quad (14)$$

and consider high energy $\epsilon \gg 1$ and strong coupling $\gamma > 1$. The time variation of the oscillator phase is given by $\dot{\psi} = -\omega - g\sqrt{2/I} \cos \psi l_x = \omega + \mathcal{O}(I^{-\frac{1}{2}})$. For sufficiently large I , and times larger than the oscillation period $\sim \omega^{-1}$ of ψ , the second term becomes negligible, i.e. we may approximate $\cos \psi \simeq \cos(\omega t + \psi(0))$. The nearly harmonic oscillation of $\cos \psi$ is exemplified by the trajectory shown in Fig. 1 (bottom left inset). It implies that the model behaves, at the high energies under consideration, much like a system of *three* dynamical variables (I, θ, ϕ) subject to external harmonic driving $\sim \cos \psi$ at a frequency ω . The spin dynamics is governed by fast precession of the angular momentum \mathbf{l} around the instantaneous rotation axis $\mathbf{\Omega} \equiv \omega_0(\gamma\sqrt{2\nu I} \cos \psi, 0, 1)^T$. For 'typical' values of $\cos \psi$, the precession frequency $|\mathbf{\Omega}| = \omega_0\sqrt{(\gamma^2 2\nu I (\cos \theta)^2 + 1)} = \mathcal{O}(\omega_0\sqrt{I}) \gg \omega$ exceeds the 'driving' frequency ω by far. This is visible in the fast spinning of the variable \mathbf{l} around the unit sphere shown in the top section of Fig. 1. Second, the precession axis is typically oriented in x -direction, $\mathbf{\Omega} \simeq \omega_0\gamma\sqrt{2\nu I} \cos \psi \mathbf{e}_x + \mathcal{O}(1/\sqrt{I})$, and during these periods the angular momentum component l_x is approximately conserved. This latter fact has important consequences for the variation of our primary variable of interest, I . Over time intervals of nearly conserved l_x , the equation of motion $\dot{I} = -\omega_0\gamma\sqrt{2\nu I} \sin \psi l_x$ can be trivially integrated to obtain the characteristic arcs visible in the bottom right panel of Fig. 1. For any particular energy set by the initial condition, the action variable varies between an upper and a lower bound (indicated by horizontal lines) calculated in Appendix C.

At times $t \sim (n\pi + \pi/2)/\omega$ (the \sim indicates a jitter of the order $1/\sqrt{I}$) the regular pattern outlined above gets interrupted, when the phase $\cos(\omega t)$ becomes small enough for $\Omega_x \sim \cos(\omega t)$ and Ω_z to be comparable. During these short time spans, the angular momentum precesses around a vector $\mathbf{\Omega}$ no longer aligned in x -direction to a new orientation (cf. the isolated arcs visible in the top part of Fig. 1.) Specifically, the x -component l_x changes to a new and essentially un-predictable value. After the time window of small $\cos \psi$ has been left, l_x is approximately conserved again and the near regular change of I re-commences, at a changed rate $\sim l_x$.

Summarizing, the system behaves as if influenced by a 'random number generator': at regular time steps $t \sim (n\pi + \pi/2)/\omega$, a new value of l_x is dialed up, and that value sets the rate at which $I(t)$ changes during the consecutive time interval of duration $\pi/2\omega$. Chaos manifests itself in this process's sensitivity to initial conditions. In the Fig. 1 this is exemplified in terms of two trajectories of slightly different initial value of the coordinate I . By comparison, Fig. 2 visualizes the profile of trajectories in the integrable realm. Notice the strongly reduced, and effectively periodic fluctuations of the ac-

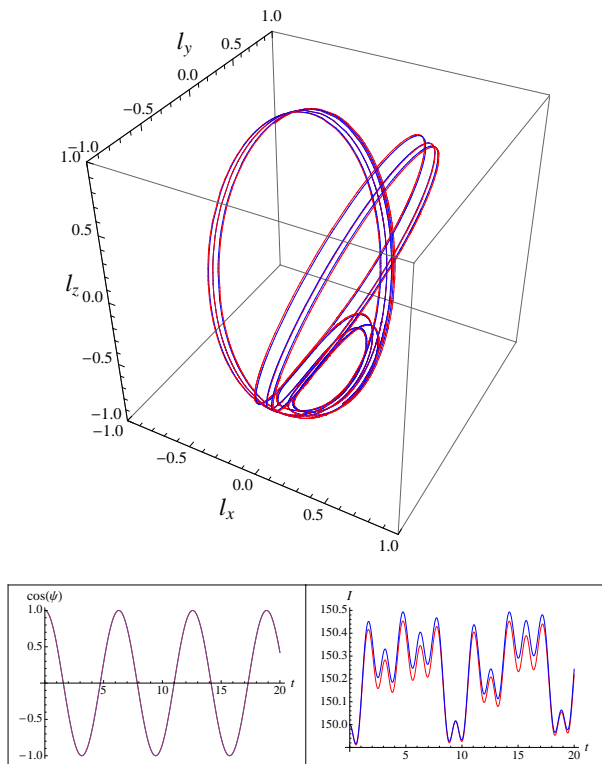


FIG. 2. Chaotic trajectories of the classical Dicke model at $g = 0.2g_c$ and $h \simeq 150\omega_0$. The red and the blue trajectory differ in a slight mismatch of the initial conditions. ♣ Note the scale on which I varies, tiny compared to the chaotic case of Fig. 1.

tion variable, and the lack of divergence of trajectories of different initial conditions.

B. Crossover to chaos

Even though the literature on the Dicke model is vast no conclusive treatment is available of the emergence of chaos as energy and coupling strength are varied. Filling that gap appears all the more desirable as much previous work is focussed on low energies where the flow cannot explore all of the spin sphere. The relative status of the superradiant phase transition at $g = g_c$ and the crossover from regular to chaotic behavior could thus not be reliably ascertained.

Global chaos is prevalent at large energies $\epsilon \gg 1$ and strong coupling $\gamma > 1$. In general, the dynamics is mixed, or, in limiting cases, integrable. To map out the regimes of different dynamical behavior, we separately consider the model at weak and high excitation energies.

Low energy dynamics. — At weak coupling $\gamma < 1$, the Dicke Hamiltonian possesses a stationary point of lowest energy $\epsilon_0 = -1$ at $I = 0$, $\cos\theta = -1$. In the energetic vicinity of this point, the dynamics is integrable. Here ‘vicinity’ means excitation energies $\Delta\epsilon \ll 1$, where $\epsilon\omega_0 = 2\omega_0$ defines the maximum energy that can

be accommodated by the spin. Integrability is visible in the Poincaré sections shown in the first few panels of Fig. 3. Signatures of mixed dynamics become visible upon approaching the critical value $\gamma = 1$. At $\gamma > 1$, the ground state configuration shifts to an energy $\epsilon_0 = -(\gamma^2 + \gamma^{-2})/2$, which is now attained at two degenerate points $(I, \psi) = \frac{1}{2\nu}(\gamma^2 - \gamma^{-2}), 0/\pi$ and $(\cos\theta, \phi) = (-\gamma^{-2}, \pi/0)$; here the non-vanishing value of the action coordinate corresponds to a macroscopic photon number $\langle a^\dagger a \rangle = jI$. In the immediate vicinity of these points, the dynamics remains integrable, and for moderate excitation it is mixed. The subsequent crossover to chaotic dynamics turns out to be rather swift; already at excitation energies $\Delta\epsilon \simeq 0.2|\epsilon_0|$, the energy shell is filled by chaotic trajectories.

High energy dynamics. — At large energies, $\epsilon \gg 1$, the Bloch sphere gets fully covered by trajectories. Already at coupling strengths $\gamma < 1$, trajectories become chaotic. The last tori get lost in the immediate vicinity of the critical value $\gamma = 1$, cf. Fig. 4.

For fully developed chaos, typical trajectories explore all of the energy shell $\epsilon\omega_0 = h$. In view of our later discussion of photon number fluctuations, we need to explore the confines of these shells, especially with regard to the coordinate I . Lower and upper bounds of the action variable can be obtained as a result of a straightforward calculation detailed in Appendix C. For large excitation energies, the accessible window of I -values asymptotes to

$$I_{\min}^{\max} = \frac{\epsilon}{\nu} \left(1 \pm \sqrt{\frac{2\gamma^2}{\epsilon}} \right), \quad (15)$$

with corrections of $\mathcal{O}(1/\epsilon)$. We are, thus, facing a window of width $\propto \sqrt{\epsilon}$ and center $\propto \epsilon$. In Section V, we will consider the ramifications of the ergodic filling of these windows in the quantum dynamics of the system.

C. Evolution of Q under chaotic drift

Focusing on global chaos from now on, we would like to clarify how the Q -function would evolve if quantum diffusion were neglected. The assumed largeness of j indeed suggests to try out that most radical implementation of the semiclassical limit.

For an initial coherent state, Q is isotropically ‘supported’ by a single Planck cell, i.e., by a tiny fraction of the energy shell located at $\langle \alpha_0, z_0 | \hat{H} | \alpha_0, z_0 \rangle = \hbar\omega_0\epsilon \propto j$ with width $\hbar\omega_0\Delta\epsilon = [\langle \alpha_0, z_0 | (\hat{H} - \hbar\omega_0\epsilon)^2 | \alpha_0, z_0 \rangle]^{1/2} \propto \sqrt{j}$. By Liouville’s theorem, that tiny fraction will not change in time. The chaotic evolution will interminably squeeze the originally ‘circular support’ of Q in the stable direction of the Hamiltonian flow and stretch it along the unstable direction. The ever narrower and longer ‘supporting stripe’ must soon begin to fold since the energy shell is compact. After a time of the order of the Ehrenfest time the stripe will have fully explored the energy shell. As the squeezing/stretching/folding of the support

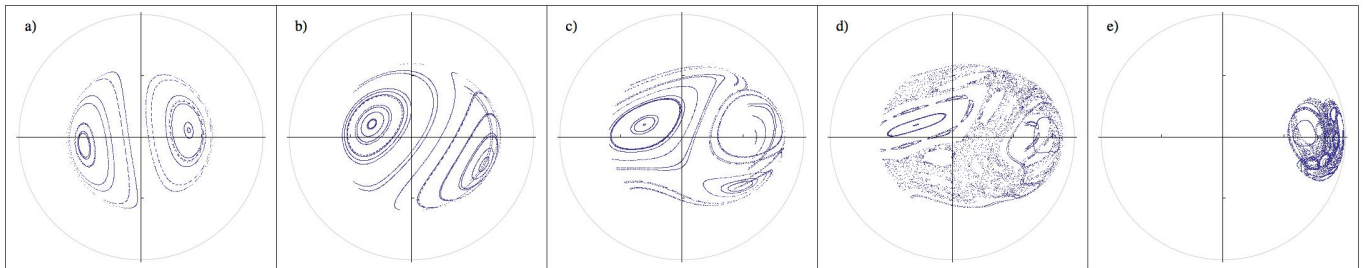


FIG. 3. Poincaré sections generated by monitoring the pair (l_x, l_y) at fixed values of the phase ψ , and at energies $\Delta\epsilon = 0.2|\epsilon_0|$ above the ground state; only southern hemisphere shown since northern one remains empty. For each parameter value, γ , nine trajectories of different on-shell initial conditions are sampled. a) $\gamma = 0.2$, b) $\gamma = 0.7$, c) $\gamma = 0.9$, d) $\gamma = 1.01$, e) $\gamma = 1.5$. What looks like crossings in (b, c) is a reflection of the non-uniqueness of $I(\epsilon, \psi, \cos\theta, \phi)$, see App. B. Noteworthy is the predominance of chaos in (e), for an energy as small as 20% of the maximum energy capacity of the spin.

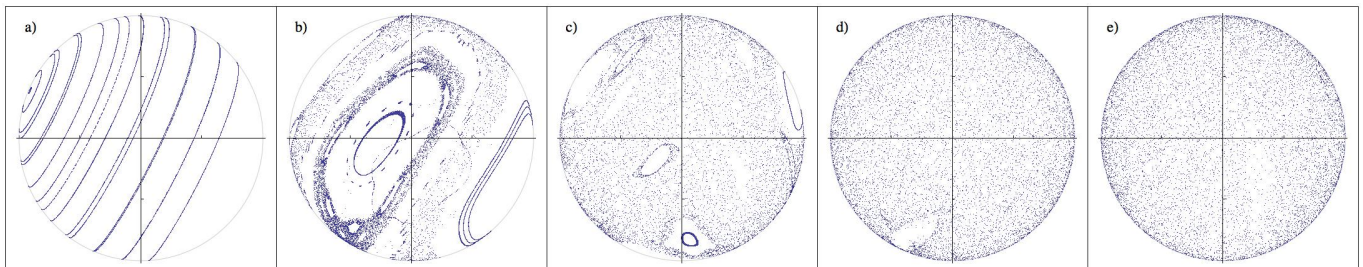


FIG. 4. Poincaré sections as in Fig. 3, now sampled at large energies $\Delta\epsilon = 30|\epsilon_0|$. Values of γ as in previous figure. The projection of the northern hemisphere, now fully covered by trajectories, looks qualitatively similar.

of Q continues, an ever finer, and eventually 'singular' structure arises, where Q alternates infinitely rapidly between high and near vanishing values transverse to the supporting stripe. Inasmuch as no region within the energy shell appears favored, a constant mean density will arise. If one were to look at the 'fissured landscape' formed by Q with finite resolution one would, from a certain time on, just observe 'flatness' at the mean value of Q mentioned. In other words, one would see the microcanonical distribution: Q constant within and zero outside the energy shell. Expectation values of observables like low-order powers of the photon number $\langle (a^\dagger a)^m \rangle$ will not register the ruggedness of Q but just 'pick up' the microcanonical shape. Somewhat cavalierly said, Q effectively equilibrates to the microcanonical distribution, within a time of the order of the Ehrenfest time.

The foregoing scenario changes little if we imagine the initial coherent state replaced by a squeezed minimum-uncertainty state. Initial states with larger uncertainties bring but two changes: (i) equilibration will happen even faster, the time scale shrinking logarithmically with the initial width, and (ii) the landscape underlying the effectively microcanonical Q can be smoother.

IV. QUANTUM DIFFUSION

Still confining ourselves to global chaos we now proceed to studying how quantum diffusion changes the effective

equilibration just found for the classical drift. We shall find a smoothing effect of quantum fluctuations which becomes effective, roughly, at phase space length scales $\sim \sqrt{\hbar}$. To the best of our knowledge, our analysis of the Dicke system represents the first case study where the interplay of quantum fluctuations and nonlinear dynamics in the long time behavior of a chaotic quantum system is resolved in concrete terms. A glance at the quantum diffusion operator (9) reveals that $\mathcal{L}_{\text{diff}}$ couples oscillator variables to spin variables but does not include second-order derivatives wrt only oscillator variables nor wrt only spin variables. That structure is of course preserved when the canonical pairs (I, ψ) and $(\cos\theta, \phi)$ are employed, as we imagine done here. A real symmetric 4×4 diffusion matrix then arises which has vanishing 'diagonal' 2×2 blocks and mutually Hermitian conjugate 'off-diagonal' 2×2 blocks, $D = \begin{pmatrix} 0 & d \\ d^\dagger & 0 \end{pmatrix}$. We shall not need the explicit dependence of the off-diagonal blocks d, d^\dagger on the variables $I, \psi \cos\theta, \phi$ here but would like to emphasize the smallness $d \propto \frac{1}{j}$.

The 'chiral' block structure of D entails a secular equation for the eigenvalues of the form $\lambda^4 - \lambda^2 \text{tr} dd^\dagger + \det dd^\dagger = 0$. The four eigenvalues of D thus come in two plus/minus pairs $\pm D_1, \pm D_2$ where D_1^2, D_2^2 are the eigenvalues of the non-negative 2×2 matrix dd^\dagger . Each of these pairs is associated with an eigenvector pair defining a contractive ($-$) resp. expansive ($+$) direction. In the expansive directions we confront normal diffusion while for

the contracting directions we may speak of anti-diffusion.

A. Qualitative discussion of equilibration

The quantum diffusive contraction (expansion) competes, given chaos, with the stretching (shrinking) inherent in the classical drift. Quantum antidiffusive shrinking will be overwhelmed by the exponential deterministic expansion in the classically unstable direction: The pertinent scales will keep growing and the corresponding structure will ever more ubiquitously explore the energy shell, much as if quantum diffusion were entirely absent. However, in the deterministically stable direction where exponential shrinking proceeds ever more slowly, quantum diffusion will not allow that shrinking to go below a quantum scale $\propto \frac{1}{\sqrt{j}}$. Therefore, the Q -function will be diffusively smoothed transverse to the unstable direction such that the deterministically favored fissured 'landscape' never arises. Microcanonical flatness will be reached from any initial state, coherent, squeezed, or broader, on the Ehrenfest time scale or faster.

The foregoing arguments do not rule out revival events,

but such cannot be expected any earlier than a Heisenberg time $t_H \propto j$, possibly even a Poincaré time ($\propto e^j$).

B. Quantitative discussion: Co-moving quantum fluctuations

The picture just drawn faithfully reflects a systematic theory obtained by projecting the dynamics onto a co-moving Poincaré section. To see that we pick a phase space point X_0 and a deflection δX . The latter may be expressed through increments of the canonical variables, $\delta X = (\delta I, \delta \psi, \delta \cos \theta, \delta \phi)^T$, or through components $(s, u, \epsilon, \tau)^T \equiv \xi$ along the four directions distinguished asymptotically by the classical flow: one stable, one unstable, and two neutrals (transverse to the energy shell and along the flow). The two variants are linearly related,

$$(\delta p, \delta x, \delta \cos \theta, \delta \phi)^T = C(s, u, \epsilon, \tau)^T, \quad (16)$$

or in brief $\delta X = C\xi$. The 4×4 matrix C is composed by the unit vectors $e_s, e_u, e_\epsilon, e_\tau$ along the stable/unstable/neutral directions as $C = (e_s, e_u, e_\epsilon, e_\tau)$; it depends on X_0 and must be determined numerically.

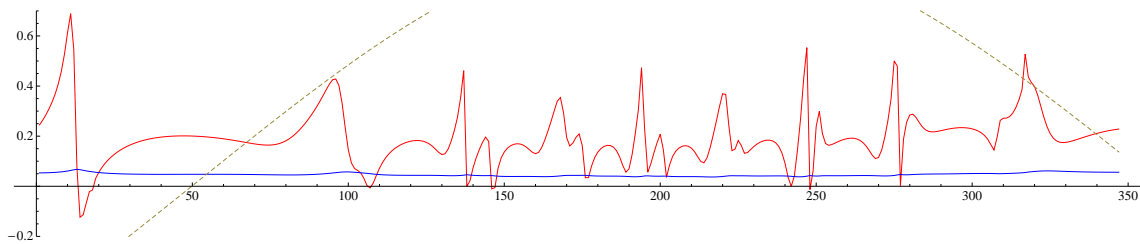


FIG. 5. (Color online) Red: the coefficient D_{ss} , Eq. (18), numerically computed along a trajectory of energy $h \simeq 250\omega_0$ and $\alpha = 1.1$. Blue: D_{ss} integrated against the Lyapunov kernel $\exp(-2\lambda t)$ as in (19). In the (arbitrary) units of the Plot, $\lambda^{-1} \simeq 150$. Dashed: the 'clock-variable' $\cos(\psi)$ effectively measuring time in units of ω^{-1} .

Now we turn to the Fokker-Planck equation for Q . Near X_0 the components of δX can be employed as $\dot{Q} = (\partial_{\delta X_i} d_i(X_0 + \delta X) + \partial_{\delta X_i} \partial_{\delta X_j} D_{ij}(X_0 + \delta X))Q$ with $d(X)$ the drift 'vector' and $D(X)$ the diffusion matrix. We then change variables according to (16) and $\partial_{\delta X} = C^T \partial_\xi$. The drift can be linearized and has the first two components $d_s = \lambda s$, $d_u = -\lambda u$ with λ the Lyapunov rate. On the other hand, in the diffusion matrix we may drop the deflection ξ . Then integrating out the variables ϵ, τ we get the bivariate density $Q(s, u)$ which obeys the reduced Fokker-Planck equation

$$\dot{Q} = (\lambda \partial_s s - \lambda \partial_u u + \partial_s^2 D_{ss} + \partial_u^2 D_{uu} + 2\partial_s \partial_u D_{su})Q. \quad (17)$$

Here the 'reduced diffusion matrix' matrix $\begin{pmatrix} D_{ss} & D_{su} \\ D_{us} & D_{uu} \end{pmatrix}$, describing quantum diffusion in the stable/unstable subspace, is the upper left 2×2 block in $C^T D C$. Intuitive

expressions arise when the orthonormal eigenvectors v_μ and eigenvalues D_μ of D are used, like

$$D_{ss} = \sum_{\mu} \langle (e_s, v_\mu) \rangle^2 D_\mu. \quad (18)$$

The sign of that effective diffusion constant will be of utmost importance. We see that the relative orientation of the intervening vectors matters, as well as the presence of positive and negative eigenvalues D_μ .

Next, we proceed from the local quantum fluctuations near X_0 to 'co-moving' fluctuations, simply following the classical trajectory starting at X_0 . Save for the replacement $X_0 \rightarrow X_t$ we have the same Fokker-Planck equation at all times t , except that the 2×2 diffusion matrix becomes time dependent along the classical trajectory. The Lyapunov rate, on the other hand, neither changes along the trajectory nor when the point X_0 is varied to

select other (infinite) trajectories [17].

The variance $\text{var}_t(s) = (\overline{s^2})_t - (\overline{s})_t^2$ of the stable deflection is readily obtained as

$$\text{var}_t(s) = e^{-2\lambda t} \text{var}_0(s) + \int_0^t dt' e^{-2\lambda(t-t')} 2D_{ss}(t'); \quad (19)$$

it must be positive at all times due to the guaranteed existence and positivity of the Q -function. In fact, to make sure we don't fall victims to our love of poetry, we have numerically checked that the diagonal element D_{ss} remains mostly positive for a large number of trajectories of varying energy and coupling parameter. An exemplary plot of D_{ss} evaluated along one of these trajectories is shown in Fig. 5. The plot exemplifies how D_{ss} only rarely turns negative. The temporal convolution with $e^{-2\lambda t}$ in (19) always entails a positive variance; see Fig. 5.

Most remarkably, the local quantum fluctuations, manifest in the directions and strengths of diffusion and antidiffusion, 'sniff out' the asymptotically stable direction e_s of the classical flow, tuning themselves to make for a positive variance $\text{var}_t(s)$ and thus a lower quantum bound $\sim \frac{1}{\sqrt{j}}$ for the scales accessible to the stable coordinate s . Co-motion is crucial since it lets the quantum fluctuations probe a time span at least of the order of the Lyapunov time, over which stability properties of the classical flow become manifest. Reassuringly, the linearization used to capture the co-moving fluctuations also remains reliable over that time span.

In the unstable direction, on the other hand, the variance $\text{var}_t(u)$ keeps growing indefinitely, as is similarly implied by the reduced Fokker-Planck equation (17). This is how the Q -function gets smoothed in the classically stable direction while forever extending its support in the unstable direction. The notorious singular structures of classical chaos are thus avoided, and equilibration to the microcanonical distribution takes place.

V. GIANT FLUCTUATIONS DUE TO CHAOS

Once more focusing on a range of energy and coupling strength with predominant classical chaos, we now turn to revealing giant fluctuations of the photon number in the stationary microcanonical regime.

If canonical pairs of variables are employed as arguments our equilibrated Q has the microcanonical form

$$Q = \frac{1}{\Omega} \delta(h - \epsilon\omega_0) \quad (20)$$

with Ω the volume of the energy shell and ϵ the (dimensionless) energy set by the initial state. That microcanonical equilibrium will of course be reached from any smooth initial state with an energy uncertainty similarly negligible as for a coherent state (where $\frac{\Delta\epsilon}{\epsilon} \sim \frac{1}{\sqrt{j}}$). Writing the delta function in the above distribution amounts to discarding corrections of relative order $\frac{1}{\sqrt{j}}$. Stationary means of powers of the photon number $\langle (a^\dagger a)^m \rangle$ for

any integer m are now accessible as moments of the microcanonical density (20). In our semiclassical situation, these means are independent of the ordering of the $2m$ factors a, a^\dagger , to leading order in j . The normally ordered form $\langle (a^\dagger)^m a^m \rangle$, measurable by absorption of the cavity output, is thus not different from the antinormally ordered form given by the moments of Q according to (6) nor from the mean powers of the photon number, $\langle (a^\dagger a)^m \rangle$, such that we have

$$\langle (a^\dagger a)^m \rangle = j^m \int_{I_{\min}}^{I_{\max}} dI \int d\psi d\cos\theta d\phi I^m \frac{\delta(h - \epsilon\omega_0)}{\Omega}. \quad (21)$$

The fourfold integral is most easily done in the case of high energies, $\epsilon > 1$, where the whole Bloch sphere is accessible (cf. Figs. 3,4). As detailed in App. D, mean and variance of the photon number then come out as

$$\begin{aligned} \langle a^\dagger a \rangle &= \left(\frac{j}{\omega}\right) \left(\epsilon\omega_0 + \frac{4g^2}{3\omega}\right) \\ \langle (a^\dagger a)^2 \rangle - \langle a^\dagger a \rangle^2 &= \frac{1}{3} \left(\frac{j}{\omega}\right)^2 \left(\frac{4\epsilon\omega_0 g^2}{\omega} + \frac{136g^4}{15\omega^2} + \omega_0^2\right). \end{aligned} \quad (22)$$

With the variance of order j^2 we indeed confront macroscopic fluctuations. Notice that to leading order, and up to numerical factors, the estimate (15) is confirmed.

We note without presenting calculations that the variance of order j^2 persists down to smaller energies, provided the energy shell is dominated by chaos. As visible in Fig. 2, $\epsilon \approx 0.2$ suffices, together with $\gamma \approx 1.5$.

VI. BEYOND THE DICKE MODEL

Evolution equations with derivatives terminating at second order are not restricted to the Dicke model. Whenever chaos is generated by a Hamiltonian of the form of a second-order polynomial in the pertinent observables and a coherent-state-based Q -function can be used, we expect a Fokker-Planck equation for Q . Examples are (i) $SU(3)$ dynamics like the Lipkin model [18], (ii) genuine many-body systems among which the Bose-Hubbard model [19, 20] is of much current interest (here the Hamiltonian is quartic in annihilation and creation operators, but due to the absence of antiresonant terms only first and second derivatives appear in the evolution equation for Q), and (iii) kicked systems like the top [17] whose near classical quantum behavior has recently been observed experimentally [21] (see Appendix E).

Even though numerous dynamical systems have Fokker-Planck equations representing their unitary quantum evolution, this behavior is by no means generic. In general, the Q -function evolves with derivatives beyond the second order. For non-polynomial Hamiltonians even infinite-order derivatives appear. The question then arises whether, given classical chaos, other equilibration mechanisms reign or whether derivatives with orders $n > 2$ give but unimportant corrections to the quantum

diffusion carried by $n = 2$. Audacious as general statements may be we dare pointing to a power counting argument which suggests prevalence of the mechanism discussed in this paper. When canonical pairs of variables are used, the generator of the time evolution of Q has the orders of derivatives and of Planck's constant interrelated as $\sum_{n=1,2,\dots} \hbar^{n-1} \partial_X^n f_n(X)$ with X and the coefficients $f_n(X)$ independent of \hbar . Herein $n = 1$ captures the classical Hamiltonian drift while $n = 2$ accounts for quantum diffusion and brings about the minimal scale $\sqrt{\hbar}$ for the stable coordinates s . We may then set $X \rightarrow X_t$ in the coefficients f_n for $n \geq 2$, integrate out all but the stable variables, and refer the stable variables to the said quantum scale as $s = \sqrt{\hbar} \tilde{s}$. A reduced generator appears as $\partial_{\tilde{s}} \lambda \tilde{s} + \sum_{n=2,\dots} \partial_{\tilde{s}}^n \hbar^{(n-2)/2} f_n(X_t)$ and indeed suggests that quantum effects are dominated by the second-order derivative terms.

Finally, inasmuch as a homogeneously filled energy shell has macroscopic extent in at least one phase space 'direction', observables exploring that direction will display macroscopic stationary fluctuations.

VII. SUMMARY AND DISCUSSION

The smoothing effect of diffusion on chaotic dynamics has been noted before, e.g., within the context of quantum billiards (cf. Ref. [22]). However, diffusive contributions to classical evolution were there added by hand. Our present analysis exemplifies how unitary quantum evolution itself brings about diffusion. By projecting the Dicke model dynamics onto a co-moving Poincaré surface of section we could check explicitly that quantum diffusion sets a limiting scale to the variance of the stable coordinate such that Q equilibrates to a smooth density of the microcanonical form.

It is well to realize that we are facing a privilege of the Q -function which other popular quasi-probability densities like the Wigner function or the Glauber-Sudarshan P -function (weight in a diagonal mixture of coherent states) do not enjoy. The Wigner function W , for instance, is known to develop positive/negative substructures within Planck cells under conditions of classical chaos [23]. Such substructures forbid pointwise convergence of W to a classical probability density as $\hbar \rightarrow 0$; they are washed out by the average over, roughly, a Planck cell which leads from W to Q . The situation is even more precarious for the P -function from which W arises by smoothing over, roughly, a Planck cell. Not only is P prone to going negative but even to loosing existence as an ordinary function under dynamics with classical chaos. For instance, a coherent initial state will get its support distorted to that of a 'Schrödinger cat state' (in the classically unstable direction) [23], which latter is known to have a non-positive and even singular P [24]. It is in fact easy to check that for the Dicke model the diffusion terms $\mathcal{L}_{\text{diff}}$ for P and Q differ only in sign (see Appendix A); therefore, the variance $\text{var}_t(s)$ which

remains positive at all times for Q must sooner or later go negative for P .

In response to the recent experimental observation of the superradiant phase transition in the Dicke model, we have investigated the prospects of detecting the concomitant transition from regular dynamics at the lowest of energies to prevalence of chaos at higher excitations. As a most interesting witness of that transition we have identified stationary fluctuations of the number of oscillator quanta (photons). While small for regular dynamics, these fluctuations rise to macroscopic magnitude as chaos proceeds towards fully covering the energy shell. Perhaps fortunately for attempts at detection, the large-fluctuation regime signalling fully chaotic behavior is found already for moderate degrees of excitation, provided the coupling is chosen above the critical value for the superradiant phase transition. The giant fluctuations are predicted to arise independent of the initial state, after a time of the order of the Ehrenfest time.

We have also argued that both our equilibration mechanism and large fluctuations of suitable observables are at work in other observable systems of current interest.

Acknowledgments — Discussions with T. Brandes, P. Braun, T. Esslinger, C. Emary, V. Gurarie, M. Kuś, J. Larson, and M. Lewenstein are gratefully acknowledged. Work supported by the SFB/TR 12 of the Deutsche Forschungsgemeinschaft.

Appendix A: Derivation of the quantum evolution equation

We start the derivation of Eq. (9) with the identity

$$\begin{aligned} \dot{Q}(\alpha, z) &= \frac{2j+1}{\pi^2(1+|z|^2)^2} \langle \alpha, z | d_t \hat{\rho} | \alpha, z \rangle \\ &= -\frac{i}{\hbar} \frac{2j+1}{\pi^2(1+|z|^2)^2} \langle \alpha, z | [\hat{H}, \hat{\rho}] | \alpha, z \rangle \\ &= -\frac{i}{\hbar} \frac{2j+1}{\pi^2(1+|z|^2)^2} \text{tr} \hat{\rho} [\hat{H}, |\alpha, z\rangle \langle \alpha, z|]. \end{aligned} \quad (\text{A1})$$

To process this expression, we need to compute the action of the Hilbert operators on coherent states. As a result of a straightforward calculation, one obtains

$$\begin{aligned} \hat{J}_- |z\rangle \langle z| &= \left(\partial_z + 2j \frac{z^*}{1+|z|^2} \right) |z\rangle \langle z|, \\ \hat{J}_+ |z\rangle \langle z| &= \left(-z^2 \partial_z + 2j \frac{z}{1+|z|^2} \right) |z\rangle \langle z|, \\ \hat{J}_z |z\rangle \langle z| &= \left(-z \partial_z + j \frac{1-|z|^2}{1+|z|^2} \right) |z\rangle \langle z|, \end{aligned} \quad (\text{A2})$$

and

$$\begin{aligned} a|\alpha\rangle \langle \alpha| &= \alpha|\alpha\rangle \langle \alpha|, \\ a^\dagger |\alpha\rangle \langle \alpha| &= (\partial_\alpha + \alpha^*) |\alpha\rangle \langle \alpha|. \end{aligned} \quad (\text{A3})$$

Substituting Eq. (1) into (A1) and using the relations above we obtain our Fokker-Planck equation (9).

Likewise, one checks that the Glauber-Sudarshan P -function, defined as the weight in the diagonal mixture of coherent states

$$\hat{\rho} = \int d\alpha dz P(\alpha, z) |\alpha, z\rangle \langle \alpha, z|, \quad (\text{A4})$$

obeys a Fokker-Planck equation whose generator differs from the one for the Q -function (cf (9)) in only two details: (i) The factor $(j+1)$ in the drift term in (9) is replaced by j . (ii) Much more importantly, the diffusion term acquires an overall minus sign.

Appendix B: Transformation to canonical variables

For completeness, we here provide a few technical details relating to the change of variables $(\alpha, \alpha^*, z, z^*) \rightarrow (I, \psi, c \equiv \cos \theta, \phi)$. The defining relations

$$z = \tan \frac{\theta}{2} e^{i\phi} = \sqrt{\frac{1-c}{1+c}} e^{i\phi} \quad \alpha = \sqrt{jI} e^{i\psi} \quad (\text{B1})$$

yield the derivatives

$$\begin{aligned} \partial_z &= -\frac{1}{2} \left[\partial_c (1+c) \sqrt{1-c^2} + i \partial_\phi \sqrt{\frac{1+c}{1-c}} \right] e^{-i\phi} \\ &\quad + \sqrt{1-c^2} e^{-i\phi}, \\ \partial_\alpha &= \left[\partial_I \sqrt{\frac{I}{j}} - \frac{i}{2\sqrt{jI}} \right] e^{-i\psi} \end{aligned} \quad (\text{B2})$$

and their complex conjugates. We must realize that the complex stereographic projection variables (z, z^*) are not a canonical pair. Therefore, a Jacobian arises in $\tilde{Q}(c, \phi, I, \psi) = \frac{2}{(1+c)^2} Q(z(c, \phi), z^*(c, \phi), \alpha(I, \psi), \alpha^*(I, \psi))$ such that to get the generator for $\tilde{Q}(c, \phi, I, \psi)$ we must replace as $\partial_c \rightarrow (1+c)^{-2} \partial_c (1+c)^2 = \partial_c + 2(1+c)^{-1}$ and

$$\partial_z \rightarrow -\frac{1}{2} \left[\partial_c (1+c) \sqrt{1-c^2} + i \partial_\psi \sqrt{\frac{1+c}{1-c}} \right] e^{-i\phi}. \quad (\text{B3})$$

Straightforward calculation then gives the generator in search as $\partial_{X_i} d_i + \partial_{X_j} \partial_{X_j} D_{ij}$ with the drift vector

$$\begin{aligned} d_I &= \sqrt{8g} \left(1 + \frac{1}{j}\right) \sqrt{I} \sin \psi \sqrt{1-c^2} \cos \phi \\ d_\psi &= \left[\omega + \sqrt{2g} \left(1 + \frac{1}{j}\right) \frac{1}{\sqrt{I}} \cos \psi \sqrt{1-c^2} \cos \phi \right] \\ d_c &= \left[-\omega_0 + \sqrt{8g} \sqrt{I} \cos \psi \frac{c}{\sqrt{1-c^2}} \cos \phi \right] \\ d_\phi &= -\sqrt{8g} \sqrt{I} \cos \psi \sqrt{1-c^2} \sin \phi, \end{aligned} \quad (\text{B4})$$

and the diffusion matrix

$$\begin{aligned} D &= \begin{pmatrix} 0 & d \\ d^\dagger & 0 \end{pmatrix}, \\ d &= \begin{pmatrix} D_{Ic} & D_{I\phi} \\ D_{\psi c} & D_{\psi\phi} \end{pmatrix} \\ &= \frac{g}{j\sqrt{2}} \begin{pmatrix} \sqrt{I} & 0 \\ 0 & \frac{1}{2\sqrt{I}} \end{pmatrix} \begin{pmatrix} A & B \\ -B & A \end{pmatrix} \begin{pmatrix} \sqrt{1-c^2} & 0 \\ 0 & \frac{1}{1-c^2} \end{pmatrix}, \\ A &= -\cos \psi \sin \phi - c \sin \psi \cos \phi, \\ B &= c \cos \psi \cos \phi - \sin \psi \sin \phi. \end{aligned} \quad (\text{B5})$$

Appendix C: Bounds on photon number in energy shell

Solving Eq. (14) for I , one readily finds

$$\frac{\sqrt{2\nu I}}{\gamma} = \pm \sqrt{(x \sin \theta)^2 + \frac{2}{\gamma^2} (\epsilon - \cos \theta) - x \sin \theta}, \quad (\text{C1})$$

where we defined $x = \cos \psi \cos \phi$. Interestingly, as a function of $\epsilon, \cos \theta, \phi, \psi$, the quantity I may take on two different values, and that complication arises when both x and $\epsilon - \cos \theta$ are negative. No solution for I exists when non-negative x meets with negative $\epsilon - \cos \theta$. The simplest situation is $\epsilon - \cos \theta > 0$: then only the positive square root in (C1) is possible and I is unique. We illustrate the search for the bounds with just a few cursory remarks on the latter case.

There is no extremum in the calculus sense. So the smallest and largest values of I must occur on the boundaries $\cos \theta = \pm 1$ or/and $x = \pm 1$. The poles of the Bloch sphere provide the "trivial" bounds $I_{\min}^{\max} = \nu^{-1}(\epsilon \pm 1)$.

To check the possibility of tighter bounds we first try $x = 1$. From $\partial \sqrt{I} / \partial \cos \theta = 0$ we get

$$\cos \theta = \frac{\gamma^2 \pm \sqrt{\gamma^4 + 1 + 2\gamma^2 \epsilon}}{1 + 2\gamma^2 \epsilon}, \quad \sqrt{I} = \frac{\gamma}{\sqrt{2\nu}} \tan \theta. \quad (\text{C2})$$

Due to $\sqrt{I} \geq 0$ and the global positivity of $\sin \theta$, we must require $\cos \theta \geq 0$ and therefore only the upper sign qualifies. A non-trivial lower bound I_{\min} is thus obtained. Similarly, the case $x = -1$ yields a non-trivial upper bound $\sqrt{I_{\max}} = -\frac{\gamma}{\sqrt{2\nu}} \tan \theta$ with $\tan \theta$ according to the lower sign in (C2). The leading terms of the ϵ -expansion of these bounds are the ones given in (15).

Appendix D: Microcanonical averages

We briefly sketch the calculation of the microcanonical moments (21), for simplicity confining ourselves to high energies ($\epsilon > 1$). Doing the I -integral in (21) we have

$$M_m \equiv \langle (aa^\dagger)^m \rangle = j^m \frac{1}{\Omega} \int d\psi d\cos \theta d\phi \frac{\hat{I}^m}{|\partial h / \partial I|_{I=\hat{i}}},$$

with the peak intensity $I = I(\psi, \phi, \theta)$ determined by (C1) and $x = \cos \psi \cos \phi$; only the positive sign in (C1) is possible at high energies. The derivative of the Hamiltonian

$$\frac{1}{|\partial h / \partial I|} = \frac{2}{\omega_0 \sqrt{2\nu\gamma}} \frac{I}{\sqrt{(x \sin \theta)^2 + \frac{2}{\gamma^2}(\epsilon - \cos \theta)}}.$$

allows to rewrite the moments as

$$M_m = \left(\frac{j\gamma^2}{2\nu}\right)^m \frac{1}{\nu\omega_0\Omega} \int d\psi d\cos\theta d\phi \frac{\left(\sqrt{(x \sin \theta)^2 + \frac{2}{\gamma^2}(\epsilon - \cos \theta)} - x \sin \theta\right)^{2m+1}}{\sqrt{(x \sin \theta)^2 + \frac{2}{\gamma^2}(\epsilon - \cos \theta)}}.$$

The power in the foregoing numerator can be binomially expanded. By symmetry only even powers of $x \sin \theta$ contribute and therefore only even powers of the square root remain. We quickly find

$$M_1 = \left(\frac{j}{\nu}\right) \left(\epsilon + \frac{1}{3}\gamma^2\right)$$

$$M_2 = \left(\frac{j}{\nu}\right)^2 \left(\epsilon^2 + \epsilon\gamma^2 + \frac{3}{10}\gamma^4 + \frac{1}{3}\right),$$

which immediately implies (22).

Appendix E: Kicked top

We would like to corroborate our expectation for the *kicked top* [18, 25], a periodically kicked large spin with conserved length, $\tilde{J}^2 = j(j+1) \gg 1$. Classical equilibration for a cloud of points on the Bloch sphere has long been known from numerical studies. Quantum equilibration and the ensuing large stationary fluctuations of the (orientation of the) angular momentum should be observable in a variant of the experiment of Ref. [21].

The simplest chaotic top has the Floquet operator

$$\hat{F} = e^{-i\frac{\tau}{2j+1}\tilde{J}_z^2} e^{-ip\tilde{J}_x};$$

it involves a rotation about the \hat{J}_x -axis by the angle p and a subsequent 'torsion' about the \hat{J}_z -axis. Torsion means a state dependent rotation by the angle $\frac{\tau}{2j+1}\hat{J}_z$ which has opposite signs in the northern and southern hemispheres. The precession angle p and the torsion constant τ are assumed independent of j . Chaos predominates if $\tau \gg 1$.

The stroboscopic time evolution of the density operator is given by $\hat{\rho}_n = \hat{F}^n \hat{\rho}_0 \hat{F}^{\dagger n}$ with the dimensionless integer 'time' n . Employing the Q -function $Q(z) = \frac{2j+1}{\pi(1+zz^*)^2} \langle z|\hat{\rho}|z\rangle$ we go for the propagator for its single-step evolution $Q_{n+1}(z) = \mathcal{F}Q_n(z)$. Like the Floquet operator \hat{F} , the Husimi propagator $\mathcal{F} = \mathcal{F}_\tau \mathcal{F}_p$ is a product of two factors, one each for precession and torsion.

For the precession we get

$$\mathcal{F}_p = \exp\left\{\frac{1}{2}ip\partial_z(1-z^2) + \text{c.c.}\right\}.$$

The generator in the foregoing exponent involves only drift (first order derivative terms) but no diffusion; it is the generator for rotation about the J_x -axis already encountered for the Dicke model in (9), classical Hamiltonian in character. The torsion propagator reads

$$\mathcal{F}_\tau = \exp\left\{-i\tau\left[\partial_z z \frac{1-zz^*}{1+zz^*} + \dots\right] + \frac{i\tau}{2j+1}\partial_z^2 z^2 + \text{c.c.}\right\},$$

with an exponent involving drift and diffusion. A $\frac{1}{j}$ -correction in the drift has not been written out. The displayed drift is again classical Hamiltonian, as becomes visible once the real canonical pair $\cos \theta, \phi$ of variables is introduced. The quantum diffusion with an explicit factor of order $\frac{1}{j}$ involves a real symmetric 2×2 diffusion matrix with vanishing diagonal elements (i. e., of chiral structure).

All arguments for equilibration for the Dicke model apply again. Most importantly, the positive eigenvalue of the diffusion matrix sets a smallest scale for the motion along the stable direction of the classical drift. On that latter scale Q becomes smooth transverse to the classically unstable direction. Effective stationarity will reign no later than about an Ehrenfest time, with Q constant over the Bloch sphere. Equipartition of Q will result in large stationary fluctuations of the angular momentum.

-
- [1] R. H. Dicke, Phys. Rev. **93**, 99 (1954)
[2] K. Hepp and E. Lieb, Phys. Rev. A **8**, 2517 (1973) Ann. Phys. (N. Y.) **76**, 360 (1973)
[3] R. Graham and M. Höhnert, Z. Phys. B **57**, 233 (1984) Phys. Lett. A **101**, 61 (1984) Phys. Rev. Lett. **57**, 1378 (1986)
[4] M. Kuś, Phys. Rev. Lett. **54**, 1343 (1985)
[5] C. Emary and T. Brandes, Phys. Rev. E **67**, 066203 (2003)
[6] K. Baumann, C. Guerlin, F. Brennecke, and T. Esslinger, Nature **464**, 1301 (2010)
[7] A. Altland and F. Haake, arXiv:1110.1270
[8] In particular, the photon operators a, a^\dagger have no clas-

- sical limit. If the Hamiltonian is written as $H = \frac{p^2}{2m} + \frac{1}{2}m\omega^2 x^2 + \omega_0 L_z + \mu x L_x$ all parameters and observables have well defined classical meanings; upon introducing $\vec{J} = \vec{L}/\hbar$ and $a = x\sqrt{\frac{m\omega}{2\hbar}} + ip\sqrt{\frac{1}{2\hbar m\omega}}$ we get the form (1) with $g = \mu\sqrt{\frac{\hbar j}{4\omega m}}$.
[9] F. T. Arecchi, E. Courtens, R. Gilmore, and H. Thomas, Phys. Rev. A **6**, 2211 (1972)
[10] R. J. Glauber and F. Haake, Phys. Rev. A **13**, 357 (1976)
[11] M. O. Scully and K. Wódkiewicz, Found. Phys. **24**, 85 (1994)
[12] R. Glauber, *Quantum Theory of Optical Coherence* (Wiley, Weinheim, 2007)

- [13] We set $(j + 1) \rightarrow j$ in the oscillator drift since the unit increment, of the same origin as the one in (7), has no further interest in the semiclassical limit. That increment would be relevant only for next-to-leading order corrections to means (of products) of the J_a .
- [14] Notice that our dimensionless action variable I differs from the standard oscillator action variable, $\tilde{I} = a^\dagger a \hbar$, by a constant factor, $I = \tilde{I}j/\hbar = \tilde{I}L$, where L is the conserved value of the classical spin angular momentum.
- [15] J. Larson and M. M. Horsdal(2010), arXiv:1009.2945
- [16] To thoroughly invalidate the rotating wave approximation, the detuning $|\omega - \omega_0|$ must exceed the natural widths of the energy levels involved.
- [17] F. Haake, *Quantum signatures of chaos, 3rd edition* (Springer-Verlag, Berlin, 2009)
- [18] S. Gnutzmann, F. Haake, and M. Kuś, J. Phys. A **33**, 143 (2000)
- [19] S. Trotzky, Y.-A. Chen, I. Flesch, A. McCulloch, U. Schollwöck, J. Eisert, and I. Bloch, arXiv:1101.2659
- [20] G. Roux, Phys. Rev. A **79**, 021608 (2009)
- [21] S. Chaudhury, A. Smith, B. E. Anderson, S. Ghose, and P. S. Jessen, Nature **461**, 768 (2009)
- [22] I. L. Aleiner and A. I. Larkin, Phys. Rev. B **54**, 14423 (1996)
- [23] W. H. Zurek, Nature **412**, 712 (2001)
- [24] H. Huang, S.-Y. Zhu, and M. S. Zubairy, Phys. Rev. A **53**, 1027 (1996)
- [25] F. Haake and M. Kus, Scholarpedia **5**, 10242 (2010)